Published in final edited form as:
Neuroscience. 2010 December 1; 171(2): 588–598. doi:10.1016/j.neuroscience.2010.08.056.

Blockade of Nerve Sprouting and Neuroma Formation Markedly Attenuates the Development of Late Stage Cancer Pain

William G. Mantyh[1,*], **Juan M. Jimenez-Andrade**[1,*], **James I. Stake**[1,*], **Aaron P. Bloom**[1], **Magdalena J. Kaczmarska**[1], **Reid N. Taylor**[1], **Katie T. Freeman**[2], **Joseph R. Ghilardi**[2], **Michael A. Kuskowski**[3], and **Patrick W. Mantyh**[1,2,4]

[1]Department of Pharmacology, College of Medicine, University of Arizona, Tucson, AZ 85724, USA

[2]Research Service, VA Medical Center, Minneapolis, MN 55417, USA

[3]GRECC, VA Medical Center, Minneapolis, MN 55417, USA

[4]Arizona Cancer Center, University of Arizona, Tucson, AZ 85724, USA

Abstract

For many patients, pain is the first sign of cancer and, while pain can be present at any time, the frequency and intensity of pain tend to increase with advancing stages of the disease. Thus, between 75 and 90% of patients with metastatic or advanced-stage cancer will experience significant cancer-induced pain. One major unanswered question is why cancer pain increases and frequently becomes more difficult to fully control with disease progression. To gain insight into this question we used a mouse model of bone cancer pain to demonstrate that as tumor growth progresses within bone, Tropomyosin receptor kinase A (TrkA)-expressing sensory and sympathetic nerve fibers undergo profuse sprouting and form neuroma-like structures. To address what is driving the pathological nerve reorganization we administered an antibody to nerve growth factor (anti-NGF). Early sustained administration of anti-NGF, whose cognate receptor is TrkA, blocks the pathological sprouting of sensory and sympathetic nerve fibers, the formation of neuroma-like structures, and inhibits the development of cancer pain. These results suggest that cancer cells and their associated stromal cells release NGF, which induces a pathological remodeling of sensory and sympathetic nerve fibers. This pathological remodeling of the peripheral nervous system then participates in driving cancer pain. Similar to therapies that target the cancer itself, the data presented here suggest that the earlier that therapies blocking this pathological nerve remodeling are initiated, the more effective the control of cancer pain.

Keywords

periosteum; breakthrough pain; preventive analgesia

In 2010, it is projected that twelve million individuals will be diagnosed with cancer and eight million will die from this disease. For many patients, pain is the first sign of cancer and

Corresponding author: Patrick W. Mantyh, Ph D, Department of Pharmacology, College of Medicine, University of Arizona, 1656 E. Mabel, Rm. #119, PO Box 245215, Tucson, AZ 85724, Phone: (520) 626-0742, Fax: (520) 626-8869, pmantyh@email.arizona.edu.
*These authors contributed equally to this study

most individuals will experience moderate to severe pain during the course of their disease (van den Beuken-van Everdingen et al., 2007). As such, cancer pain not only causes significant suffering but contributes to a decreased quality of life, functional status, and greatly increases health care utilization.

Cancer pain is commonly divided into three categories: ongoing pain, spontaneous breakthrough pain, and movement-evoked breakthrough pain (Portenoy and Hagen, 1990, Mercadante and Arcuri, 1998). Ongoing pain, which is the most common form of cancer pain and is frequently the first sign of cancer, usually begins as a dull, aching pain that increases in intensity with time (Portenoy and Lesage, 1999). With disease progression, intermittent episodes of breakthrough pain can occur either spontaneously or with movement of the tumor-bearing organ (Mercadante, 1997, Portenoy and Lesage, 1999, Mercadante et al., 2004). This pain is referred to as breakthrough pain as it “breaks through” the analgesic regimen controlling the ongoing cancer pain. Of all cancer pains, breakthrough pain is generally the most difficult to fully control, as this pain can be severe, sudden in onset (seconds – minutes), and can occur several times per day. Additionally, the dose of opioids required to fully control this pain is generally significantly higher than that required to control ongoing pain, and administration of high doses of opioids is often accompanied by unwanted side effects such as sedation, somnolence, depression, cognitive impairment, respiratory depression, and constipation (Mercadante, 1997, Portenoy, 1999).

In the past decade there has been progress in understanding some of the mechanisms that drive ongoing cancer pain, which include sensitization of nociceptors by algogenic products released from tumor and associated stromal cells, acidosis, injury, and destruction of nerve fibers by tumor cells and hypoxia (Schwei et al., 1999, Ghilardi et al., 2005, Peters et al., 2005, Sevcik et al., 2005a, Sevcik et al., 2005b, Mantyh, 2006). What remains largely unknown is why cancer pain usually increases with time and what may drive spontaneous and/or movement evoked breakthrough cancer pain. One largely unexplored possible mechanism that could drive cancer pain is that nerve fibers are not merely static structures that simply respond to the changing tumor environment, but rather can undergo actively and pathological remodeling. This pathological reorganization of nerve fibers would then set in place a neuroanatomical substrate that would not only be highly sensitive to movement of the tumor-bearing organ but also create an “ectopic generator” which could spontaneously discharge with accompanying pain.

Here we provide evidence, using an established model of cancer pain, that sensory and sympathetic nerve fibers can undergo a profound and pathological reorganization which, in other pain states, is known to give rise to severe movement evoked and spontaneous chronic pain. This pathological sprouting and neuroma formation appears to be driven by NGF, as sequestration of NGF using an anti-NGF antibody largely blocks this pathological reorganization and inhibits the development of severe cancer pain.

Experimental Procedures

Culture and injection of tumor cells

All procedures were approved by the Institutional Animal Care and Use Committee at the Minneapolis VA Medical Center (Minneapolis, MN) and the University of Arizona (Tucson, AZ). All efforts were made to minimize the suffering and number of animals used. A total of 70 mice were evaluated in this study, 43 of which were injected with osteolytic murine sarcoma cells (NCTC 2472) stably transfected with green fluorescent protein (GFP). These cancer cells were injected into the femoral intramedullary space (left femur) of male C3He/HeJ mice (8 weeks old, Jackson) according to previously described protocol (Sevcik et al., 2004, Sevcik et al., 2005b). Following induction of general anesthesia with

ketamine:xylazine (100 mg/kg/5 mg/kg, i.p.), an arthrotomy was performed exposing the condyles of the distal femur. The bone was cored with a 30 gauge needle inserted at the level of the intercondylar notch. The coring needle was then replaced with a 29 gauge hypodermic needle used to inject either Hank's buffered sterile saline as the control (HBSS, Sigma, 20μl) or HBSS containing 10^5 sarcoma cells (20μl) into the intramedullary space. In order to prevent cell reflux following injection, the injection site was sealed with dental grade amalgam (Dentsply) using an endodontic messing gun (Union Broach), followed by copious irrigation with sterile filtered water (hypotonic solution). Wound closure was achieved using a single 7mm auto wound clip (Becton Dickinson).

Anti-NGF treatment

The anti-NGF sequestering antibody (mAb 911, Rinat/Pfizer), is effective in blocking the binding of NGF to both TrkA and p75 NGF receptors and inhibiting TrkA autophosphorylation (Hongo et al., 2000). The anti-NGF antibody possesses a plasma half-life of approximately 5-6 days in the mouse and it does not appreciably cross the blood brain barrier (Shelton et al., 2005). The dose used (10 mg/kg) was based on previous studies (Halvorson et al., 2005, Sevcik et al., 2005b) and delivered by intraperitoneal injection (i.p.). Therapy regimens were initiated either when cancer-induced pain behaviors became evident (day 6) or after significant disease progression (day 18). Sarcoma-bearing mice were divided into 4 groups: sarcoma + vehicle, sarcoma + early/acute anti-NGF treatment (10 mg/kg; i.p., given at day 6 post cell injection), sarcoma + early/sustained anti-NGF treatment (10 mg/kg; i.p., given at days 6, 12, and 18 post cell injection), and sarcoma + late/acute anti-NGF treatment (10 mg/kg; i.p., given at day 18 post cell injection). The animals were gently held by the scruff while i.p. injection of anti-NGF was performed. To compare the magnitude of the analgesic effect in the groups, the number of nociceptive behaviors was expressed as % nociception, where 100% nociception was defined as the number of flinches in the sarcoma + vehicle group.

Behavioral analysis

Mice were behaviorally tested at days 8, 10, 12 14, 16, 18, and 20 post-cell or HBSS (vehicle) injection. Mice were placed in a clear plastic observation box with a wire mesh floor and allowed to habituate for a period of 30 min. After acclimation, the number of spontaneous flinches and the time spent guarding the tumor-bearing limb were recorded over a 2 minute period. Flinches were defined as the number of times the animal raised its hindpaw aloft while not ambulatory. Guarding was defined as the time the hindpaw was held aloft while ambulatory. The investigator was blinded as to the experimental condition of the animals.

Radiographic analysis of tumor-induced bone destruction

After behavioral analysis, mice were lightly anesthetized (2% isoflurane) and digital radiographs (MX20 DC12, Faxitron XRay) of lower extremities were obtained. Radiograph images of the medial-lateral plane of both bones were used to evaluate tumor-induced bone destruction as previously performed (Honore et al., 2000). Radiographs of tumor-bearing femora were used to evaluate bone destruction and were assigned scores of 0–4: 0, normal bone with no signs of destruction; 1, small radiolucent lesions indicative of bone destruction (one to three lesions); 2, increased number of lesions (three to six lesions) and loss of medullary bone; 3, loss of medullary bone and erosion of cortical bone; 4, full-thickness unicortical bone loss. Analysis was performed in a blinded fashion.

Euthanasia

At day 20 post sarcoma cell injection, mice were sacrificed using CO_2 delivered from a compressed gas cylinder and perfused intracardially with 20 ml of 0.1M phosphate buffered saline (PBS, pH=7.4 at 4°C) followed by 20 ml of 4% formaldehyde/12.5% picric acid solution in 0.1M PBS (pH=6.9 at 4°C). Unlike our previous work involving therapeutic administration of anti-NGF (Sevcik et al., 2005b) in which the mice were sacrificed at day 14 post-cancer injection, mice were sacrificed at day 20 following cancer cell injection in the present study. This change was incorporated due to the observation that although at day 12 the osteolytic sarcoma cells began to migrate from the marrow space via nutrient foramens, inducing microfractures and cortical lesions, an extended experimental period allowed a more comprehensive examination of nerve fiber sprouting and neuroma formation

After sacrifice and perfusion, mouse femurs were removed, post-fixed for 4 hours in the perfusion fixative and placed in PBS solution at 4°C.

Micro-computed tomography (μCT) analysis

In order to characterize disease progression and cancer-induced changes in mineralized bone micro architecture, femurs were analyzed with an eXplore Locus SP micro-computed tomographer (μCT, GE Healthcare). This conebeam μCT scanner uses a 2300 × 2300 CCD detector with current and voltage set at 80 μA and 80 KVp, respectively. Specimens were scanned in 1080 views through 360° with a 2100 ms integration time. Scans were then reconstructed at 16-μm^3 resolution using Reconstruction Utility software (GE Healthcare). μCT parameters used to assess disease progression and cancer-induced bone deterioration included cortical thickness, bone mineral density, trabecular number, and Bone Volume / Tissue Volume (BV/TV).

Immunohistochemistry

Femurs were harvested and processed for immunohistochemistry, and were visualized either as periosteal whole mounts (bird's eye view of the periosteum) or as frozen sections (lateral/ cross-sectional view). Of the 70 total mice evaluated in the present report, 37 were used for whole mount preparations.

For whole mount preparations, periosteum from the left diaphyseal shaft was removed and processed for immunohistochemistry according to the following procedure adapted from previous studies (Mach et al., 2002). Briefly, excess muscle was carefully removed from the femur using surgical scissors without disturbing the bone and attached periosteum. Periosteum was harvested from the distal growth plate region to immediately below the third trochanter. Periosteum was removed from the bone by tracing the lower and upper limits of the desired area with a micro scalpel blade and a vertical cut was then performed along the posterior surface of the bone. Under a dissecting microscope, the periosteum was removed by gently scraping against the bone using the edge of forceps (Brownlow et al., 2000). In our hands, the technique described above resulted in maximal preservation and minimal damage to both the cambium and fibrous layers of the periosteum. During periosteum removal, femurs were continually irrigated with PBS to prevent tissue dehydration. The size of the periosteal whole mount preparation and its attached thin muscle layer used for immunohistochemistry was approximately: width=6 mm; length=6 mm; thickness=0.5 mm.

Preparations were blocked with 3% normal donkey serum for 1 hr and incubated with primary antibodies overnight. Peptide-rich sensory nerve fibers were labeled with rabbit anti-CGRP (1:12,000; Sigma) (Lawson et al., 1993). Myelinated primary sensory nerve fibers were labeled with chicken anti-NF200 (1:1000; Chemicon) (Lawson and Waddell, 1991). Post-ganglionic sympathetic nerve fibers were labeled with rabbit anti-tyrosine

hydroxylase (TH, 1:1000; Chemicon). Nerve fibers positive for tropomyosin receptor kinase A (TrkA) were labeled with goat anti-TrkA (1:100; R&D). Since endogenous GFP signal from cancer cells was visualized in the FITC channel, preparations were then incubated with Cy3- and Cy5-conjugated secondary antibodies (1:600; Jackson ImmunoResearch) for 1 hr. For double immunofluorescence, preparations were incubated with a mixture of primary antibodies followed by a mixture of Cy3 and Cy5-conjugated secondary antibodies.

Preparations were then washed with PBS three times and counterstained with DAPI (4′, 6-diamidino-2-phenyl-indole, dihydrochloride, 1:30000, Molecular Probes, OR, USA) for 5 minutes and washed with PBS. Finally, tissue was dehydrated through an alcohol gradient (70, 80, 90, and 100%), cleared in xylene, mounted (with attached muscle layer in contact with the slide) on gelatin-coated slides, and coverslipped with di-n-butylphthalate-polystyrene-xylene (Sigma). Preparations were allowed to dry at room temperature for 12 hours before imaging.

To view the lateral/cross-sectional areas of periosteum attached to the bone, decalcified frozen sections of the left femur were obtained. Of the total 70 mice, 33 were used for frozen sections. Mouse femurs were gently decalcified in 10% EDTA, for ~2 weeks, at which point, as evaluated by radiographic analysis, the femur reaches the minimum decalcification necessary for cryostat sectioning. Femurs were then cryoprotected by immersion in a 30% sucrose solution for 48 hours, and then serially sectioned along the longitudinal axis at a thickness of 30 μm. Frozen cross-sections were stained with the same methodology and antibodies used for whole mount preparations.

Laser Confocal Microscopy

The Olympus Fluoview FV1000 system used in the present study is equipped with different lasers (Multiline Argon (458 nm, 488 nm, 515 nm), Green HeNe (543 nm), Red HeNe (633 nm), and Blue Diode (405 nm)) and multiple excitation and emission fluorescence filters. The endogenous GFP signal emitted by the sarcoma cells did not require amplification for analysis. The GFP expression was visualized by using an excitation laser beam of 488 nm wavelength, and emissions were detected using a 522 nm emission filter. Sequential acquisition mode was used to reduce bleed-through.

For whole mounts, confocal images were obtained from the mid-diaphysis. Images were projected from 280 optical sections at 0.25μm intervals with a 40× objective. For frozen sections, images were acquired in the proximal metaphyseal periosteum (~2 mm below the growth plate). Confocal images of frozen sections were acquired from sections 30 μm in thickness and were projected from 120 optical sections at 0.25 μm intervals with a 40× objective.

The 3D renderings of bone with overlaid nerve fibers were assembled and created with the use of Amira software. For each 3D rendering, four 40× confocal images were acquired and overlaid, to scale, on top of the image's corresponding bone, which was rendered using μCT slices compiled with Amira software.

Sprouting and neuroma quantification

For quantification, frozen sections were used, as the cross sections allow visualization of the bone's landmarks (such as the growth plate), which enable the observer to locate the same anatomical area when quantifying different animals. The number of animals used for frozen section analysis was: n=8 for sham + vehicle, n=9 for sarcoma + vehicle, n=9 for sarcoma + early/sustained anti-NGF, and n=7 for sarcoma + late/acute anti-NGF.

For each femur, we obtained approximately 32 separate frozen sections, each section being cut at 20 μm. For each given marker, 3 images were obtained. Each image was acquired 2 mm from the proximal growth plate, with images taken from different sections at least 0.1 mm apart. The area of periosteum that was analyzed was an average 620 μm (length), 70 μm (width), and 20 μm (depth). The Z-stacked images were analyzed with Image-Pro Plus v. 6.0 (Media Cybernetics) and nerve fibers were manually traced to determine the length of nerve fibers. In each image the area of the periosteum was determined using the built-in area tool. Nerve sprouting was reported as total length of nerve fibers per volume of periosteum (Yen et al., 2006).

To quantify the extent of formation of neuroma-like structures, frozen sections were examined with a fluorescent microscope and these structures were manually counted and totaled from the entire 30μm-thick section. Three different sections, each at least 0.1 mm apart, were evaluated per animal. A neuroma-like structure, was defined as satisfying all 3 of the following characteristics, i.) a disordered mass of blind ending axons ($CGRP^+$, $NF200^+$, or TH^+) that has an interlacing and/or whirling morphology, ii.) a structure with a size of more than 10 individual axons that is at least 20 μm thick and 70 μm long, and iii.) a structure that is never observed in the periosteum of normal bone (Devor and Wall, 1976, Sung and Mastri, 1983).

Statistical analysis

Data are presented as mean ± SEM. Immunohistochemical and pain behavioral data were analyzed across treatment groups using a Kruskal-Wallis nonparametric analysis of variance. Significant main effects of groups were followed by Mann-Whitney nonparametric t-tests with Bonferroni adjustment for multiple comparisons.

Results

Tumor growth induces exuberant sprouting of sensory and sympathetic nerve fibers and the formation of neuroma-like structures

In the present report, tumor-induced changes were examined in the periosteum, as this bone compartment is richly innervated by sensory and sympathetic nerve fibers (Mach et al., 2002) and appears to be pivotally involved in detecting injury to the skeleton (Inman, 1944, Greenfield, 2006). Additionally, the periosteum is the only bone tissue that can be immunohistochemically analyzed in both decalcified frozen sections and non-decalcified whole mount preparations (Jimenez-Andrade et al., 2010). In comparing the organization and density of $CGRP^+$ (Figs. 1A, 2A), $NF200^+$ (Fig. 3A), or TH^+ (Fig. 3D) periosteal nerve fibers across the naïve and sham operated groups, there did not appear to be any difference in naïve vs. sham operated mice (data not shown). What is clear, however, is that in both naïve and sham operated mice, the organization and density of $CGRP^+$ and $NF200^+$ nerve fibers is very different from TH^+ sympathetic nerve fibers. Thus, whereas $CGRP^+$ and $NF200^+$ sensory nerve fibers have a net-like organization and are not closely associated with blood vessels, TH^+ sympathetic nerve fibers innervate and wrap blood vessels in a tight corkscrew-like fashion.

Six days following tumor injection into the intramedullary space of the mouse femur, we observed significant osteoclast-mediated bone resorption, the first signs of osteolytic lesions, and significant bone cancer pain. By 12 days post-tumor injection, GFP^+ tumor cells had completely filled the intramedullary space and, either via growth through the nutrient foramen or tumor induced micro-fracture of the bone, GFP^+ tumor cells had begun to grow between the outside of the cortical bone and the overlying periosteum as revealed by immunohistochemical analysis (data not shown). By 20 days post-tumor injection, we

observed significant sprouting and formation of neuroma-like structures by $CGRP^+$ (Figs. 1B, 2B), $NF200^+$ (Fig. 3B), and TH^+ (Fig. 3E) nerve fibers. Sprouting $CGRP^+$, $NF200^+$, and TH^+ nerve fibers appeared to be intermingled amongst themselves, the GFP^+ tumor cells, and $CD68^+$ tumor-associated macrophages. It should be noted that in the tumor-bearing tissue not only was there an increased density of $CGRP^+$, $NF200^+$, and TH^+ nerve fibers, but also a highly pathological and disorganized pattern of innervation that is never observed in the periosteum of naïve or sham operated mice.

Whereas 100% of GFP^+ sarcoma injected mice treated with vehicle showed significant sprouting of $CGRP^+$, $NF200^+$, and TH^+ nerve fibers, approximately 50% of these mice had 1-2 neuroma-like structures in the periosteum (Fig. 1, B and D). These neuroma-like structures appear as a disordered mass of blind ending axons that have an interlacing or whirling morphology and are never observed in sham or naïve animals. Previous studies have shown that neuromas frequently form after nerve injury and are comprised of both sensory and sympathetic nerve fibers (Small et al., 1990, Lindqvist et al., 2000). Given that our antibodies for sympathetic nerve fibers (TH) and sensory nerve fibers (CGRP) are raised in the same species, co-localization experiments were not possible. However in serial sections of tumor-bearing periosteum consecutively stained for $CGRP^+$ (Fig. 4A), $NF200^+$ (Fig. 4B), and TH^+ (Fig. 4C), all three populations of nerve fibers appear to be present in the same neuroma-like structure (Fig. 4D). In order to rule out the possibility that the overlap between myelinated and unmyelinated fibers in this model is due to hypertrophy of sympathetic fibers, which is accompanied by a myelination of peripheral fibers, we performed co-localization experiments of TH and NF200 in both normal and tumor bearing bones. While both antibodies provide robust staining, we have never observed NF200 staining in TH^+ nerve fibers or TH staining in $NF200^+$ nerve fibers.

Early sequestration of NGF attenuates tumor-induced nerve sprouting and formation of neuroma-like structures

To begin to define what factor(s) might drive the sprouting and neuroma formation of $CGRP^+$, $NF200^+$, and TH^+ nerve fibers, we used double-label immunohistochemistry with an additional antibody to TrkA. While the majority of $CGRP^+$ and TH^+ cell bodies, as well as some $NF200^+$ cell bodies, have been shown to colocalize with TrkA (Averill et al., 1995, Schmidt et al., 1998), nearly all the sprouting $CGRP^+$ (Fig 2B, 2E), $NF200^+$ (Supplemental figure 1) and TH^+ (data not shown) nerve fibers expressed TrkA (Fig. 2, D to F).

In light of these findings, and given that TrkA is the cognate receptor for NGF (Pezet and McMahon, 2006), we treated sarcoma-injected mice with a highly specific NGF sequestering therapy (anti-NGF) (Hongo et al., 2000). Data from these studies demonstrated that early/sustained treatment with anti-NGF (given at 6, 12 and 18 days post tumor injection) significantly attenuated the sprouting of $CGRP^+$ (Fig. 2C), $NF200^+$ (Fig. 3C), and TH^+ (Fig. 3F) nerve fibers. Interestingly, significant attenuation of this sprouting was only observed with the early/sustained anti-NGF administration but not with late/acute administration (given once at day 18 post tumor injection) (Fig. 5, A to C). Early/sustained administration of anti-NGF similarly resulted in a marked decrease in the formation of neuroma-like structures whereas in the late/acute administration group, as many as 50% of the animals examined had $CGRP^+$, $NF200^+$, and TH^+ neuroma-like structures. Importantly, early/sustained administration of anti-NGF did not affect the organization or density of $CGRP^+$, $NF200^+$, or TH^+ fibers in the contralateral, non-tumor bearing bones compared to sham mice (Table 1). Additionally, in agreement with previous *in vivo* studies, anti-NGF therapy had no effect on disease progression as measured by tumor growth within or outside the marrow space, tumor-induced bone destruction/remodeling, or tumor metastasis (Halvorson et al., 2005, Sevcik et al., 2005b).

Early, but not late sequestration of NGF attenuates tumor-induced pain

To assess whether the observed aberrant nerve growth correlates with increasing cancer pain, and to determine whether anti-NGF therapy attenuates this pain, pain behaviors were analyzed in tumor-bearing mice treated with early/acute anti-NGF (anti-NGF administered once at day 6), early/sustained anti-NGF (anti-NGF administered at day 6, 12, and 18), and late/acute anti-NGF (anti-NGF administered once at day 18), and compared to sham animals treated with vehicle. These behavioral analyses showed that at early time-points (days 8–12 post tumor cell injection), pain-related behaviors gradually increased with time (Fig. 6A), and correlate with tumor growth in the intramedullary space of the femur, as well as progressive tumor-induced bone destruction. Interestingly, pain behaviors appear to escalate more rapidly upon the escape of sarcoma cells from the intramedullary space (days 12–20 post tumor injection) (Fig. 6A), which correlates with tumor-induced sprouting of $CGRP^+$, $NF200^+$, and TH^+ nerve fibers (Figs. 1B, 2B, 3B and D). Behavioral analysis revealed that when anti-NGF was given at day 6 post tumor injection, pain behaviors are reduced by ~40% by day 8, whereas early/sustained administration of anti-NGF from days 6-18 reduced pain behaviors by ~60% at day 20. In contrast, when anti-NGF was administered late (on day 18), it did not produce a statistically significant reduction in cancer pain behaviors at day 20 (Fig. 6B).

Discussion

In the present report we use a mouse model of bone cancer pain (Schwei et al., 1999, Brainin-Mattos et al., 2006, King et al., 2007) to show that sensory and sympathetic nerve fibers innervating bone undergo a remarkable and pathological reorganization that appears to significantly contribute to cancer pain. In particular, we have shown that when GFP^+ tumor cells growing within the bone marrow escape and invade the periosteum, a rapid and ectopic sprouting of $CGRP^+$ and $NF200^+$ sensory, and TH^+ sympathetic nerve fibers occurs in the periosteum. These newly sprouted nerve fibers are intermingled amongst themselves, the tumor cells, and their associated stromal, inflammatory, and immune cells. Interestingly, this dense and disorganized appearance of sensory and sympathetic nerve fibers is never observed in normal bone. These data are supported by previous findings that show that when provided with the appropriate trophic factor, even adult sensory and sympathetic nerve fibers can grow at a remarkable pace, sprouting several millimeters a day (Cohen et al., 1954, Madduri et al., 2009). In addition to the exuberant sprouting of $CGRP^+$ nerve fibers, in approximately 1 out of 2 tumor-bearing, vehicle treated bones we observe the appearance of occasional but highly recognizable neuroma-like structures. In all cases the neuroma formation occurred when the tumor cells had reached the periosteum. Whether the mechanisms that induce nerve sprouting versus neuroma formation are similar or different is unknown, and future studies are clearly needed to answer this question. As previously described for neuromas in both animals and humans, these neuroma-like structures appear as a disordered mass of blind ending axons that have an interlacing or whirling morphology (Devor and Wall, 1976, Sung and Mastri, 1983) and are not observed in the sham vehicle-treated or naïve bone. Previous studies have shown that injury to peripheral nerves associated with trauma, amputation, compression, or surgery can lead to painful neuromas (Devor and Govrin-Lippmann, 1983, Lindqvist et al., 2000, Kryger et al., 2001, Black et al., 2008), which have a morphology similar to the neuroma-like structures observed in the present tumor-bearing mouse bones. In humans, these non-malignant neuromas frequently cause chronic and severe pain (Lindqvist et al., 2000, Devor, 2001, Black et al., 2008), produce spontaneous ectopic discharges (Nystrom and Hagbarth, 1981, Devor and Govrin-Lippmann, 1983, Devor et al., 1990) in part by up-regulation of sodium channels (Devor et al., 1993, England et al., 1996, Black et al., 2008), and are largely refractory to medical treatment (Black et al., 2008). Whether these neuroma-like structures in the tumor-bearing

bone also show an up-regulation of sodium channels and produce spontaneous discharges is unknown, but these structures could partially explain the phenomenon of spontaneous breakthrough cancer pain, as movement would not be required for these spontaneous ectopic and painful discharges to occur.

In the normal bone neither unmyelinated and thinly myelinated ($CGRP^+$) (Lawson et al., 1993) and myelinated ($NF200^+$) (Lawson and Waddell, 1991) nerve fibers are usually found in close contact with TH^+ sympathetic nerve fibers. Thus, whereas the sensory nerve fibers are generally not closely associated with blood vessels that vascularize bone, sympathetic TH^+ fibers show a striking innervation of blood vessels by tightly ensheathing blood vessels in a “corkscrew”-like pattern. In contrast, in areas where there is extensive tumor induced nerve sprouting or neuroma formation, $CGRP^+$, $NF200^+$, and TH^+ nerve fibers all appear to have a similar disorganized pattern and appear to be intermingled amongst each other. While we do not yet know whether areas of intense nerve sprouting eventually become neuromas, in the few cases where we have been able to obtain consecutive serial sections of $CGRP^+$, TH^+, and $NF200^+$ from the same neuroma, all three populations of nerve fibers appear to be present. This is of significant interest, as one mechanism that is thought to generate and maintain pain in complex regional pain syndrome (CRPS) is an aberrant sprouting of sympathetic nerve fibers, such that noradrenaline released from sympathetic nerve fibers now excites nearby sensory nerve fibers (Janig and Baron, 2003). As we observe a similar intermingling of sensory and sympathetic nerve fibers in areas of dense sprouting and neuroma-like formation in tumor-bearing bones, this pathological intermingling of sensory and sympathetic nerve fibers may provide an anatomical substrate that drives a sympathetically maintained cancer pain.

To address the question of what factors might be driving the sprouting and formation of neuroma-like structures, we focused on the NGF/TrkA axis, as in the tumor-bearing mice the great majority of $CGRP^+$ and $NF200^+$ nerve fibers that undergo sprouting also express TrkA. Previous reports have exhaustively demonstrated that in both the developing and adult animal, NGF can induce marked sprouting of $TrkA^+$ sensory and sympathetic nerve fibers (Pezet and McMahon, 2006). Using a mouse monoclonal antibody against NGF (anti-NGF) (Hongo et al., 2000), we show that while early and sustained administration of anti-NGF results in a marked reduction of sprouting and neuroma-like formation by $CGRP^+$, TH^+, and $NF200^+$ nerve fibers in the tumor-bearing bone, this treatment does not reduce the density of normal nerve fibers in the contralateral, non-tumor-bearing bone. Whether NGF drives this sprouting through binding to the TrkA or p75 receptor is as yet unknown, but other studies suggest that TrkA is more involved in driving sprouting (Gallo et al., 1997) while p75 is more involved in apoptosis (Bamji et al., 1998). The precise contributions of these two receptors in these processes, however, remain unclear.

A key unknown is the source of the NGF that appears to be driving the sprouting of sensory nerve fibers and ultimately the pain in the tumor-bearing tissue. Sarcoma cells of the type used here produce small but significant amounts of NGF (Cohen et al., 1954, Sevcik et al., 2005b), suggesting that the tumor may be the primary source of NGF. However, a canine prostate cell line (ACE-1) that does not express any identifiable NGF mRNA (Halvorson et al., 2005) also induces significant bone cancer pain and nerve sprouting that is reduced by treatment with anti-NGF (unpublished data). These data, together with significant literature suggesting that macrophages, neutrophils, endothelial cells, T-lymphocytes, and fibroblasts can all express significant levels of NGF, suggest that most of the NGF produced in cancers arises from tumor-associated inflammatory, immune, and stromal cells rather than from the tumor itself (Lindsay et al., 2005, Pezet and McMahon, 2006). This is not surprising in light of the fact that in most cancers, 10-60% of the tumor mass is composed of these tumor-associated cells (Normann, 1985, Bingle et al., 2002).

To evaluate the effect of acute or chronic dosing of anti-NGF on pain-related behaviors, these behaviors were evaluated in early stages of disease progression at day 8 (after anti-NGF was begun at day 6) and at late stages of disease progression at day 20 (after anti-NGF administration was begun at day 6 or day 18). When anti-NGF administration was begun at day 6 post-tumor injection there was a 40 and 60% reduction when pain behaviors were assessed at days 8 and 20, respectively. In contrast, when anti-NGF was administered late in disease progression at day 18 and pain behaviors assessed at day 20 (when ectopic spouting and neuroma formation had already occurred) there was no significant reduction in pain-related behaviors. It should be noted that a mouse fracture pain model showed that when the anti-NGF therapy was administered at day 1 following fracture, when the pain was severe but nerve sprouting had yet to occur, anti-NGF achieved full analgesic efficacy (a 50% reduction in pain) one day following initial administration (Jimenez-Andrade et al., 2007). Together, these data suggest that once robust sprouting and neuroma formation has occurred, the same dose of anti-NGF that effectively reduced severe pain before the pathological reorganization no longer has potency after the reorganization has occurred. Interestingly, the present data fits well with previous data suggesting that whereas anti-NGF is highly efficacious at inhibiting the regeneration of sensory nerve fibers, anti-NGF showed little if any efficacy at “trimming back” or “pruning” nerve fibers once regeneration had occurred (Diamond et al., 1992). It should be noted that previous studies in our lab have shown that anti-NGF therapy is effective at reducing the pain-related behaviors even before the appearance of nerve sprouting and neuroma-like structures. Furthermore, it is important to note that in the present study, animals treated with anti-NGF still display some, albeit reduced, nociceptive behaviors. In light of this, we believe that NGF is involved in sensitizing $TrkA^+$ sensory nerve fibers and driving nerve sprouting and neuroma formation. However, even in the absence of NGF, tumor-induced acidosis, mechanical distortion of sensory nerve fibers, release of algogenic substances such as bradykinin, endothelin, prostaglandins and proteases all contribute to driving bone cancer pain (Mantyh, 2006). Thus, while NGF is an important player in driving bone cancer pain, it is certainly not the only player.

The present data suggest that at least in bone cancer pain, anti-NGF produces optimal analgesic efficacy when administered early, before the development of a chronic pain state, a concept known as preventive analgesia. Although the concept of preventive analgesia is both intuitive and appealing, its scientific basis is largely unknown. For example, whereas preventive analgesia has been demonstrated in animal models, with experiments showing that blockade of early pain reduces synaptic strengthening of pain circuits in the spinal cord and brain (Woolf and Chong, 1993), human clinical trials have been equivocal (Pogatzki-Zahn and Zahn, 2006). It remains unclear whether this failure is caused by problems with the definition of preventive analgesia, the design of the studies, the specific types of pain that have been targeted, or whether there really is no clinical benefit to preventive analgesia (Ballantyne, 2001). However, the present study identifies a potential anatomical substrate by which blockade of the NGF/TrkA axis could produce a clear preventive analgesic effect. Previous studies have shown that inappropriate remodeling of sensory and sympathetic nerve fibers, whether it be sprouting or neuroma-like formation, can give rise to hyperalgesia, allodynia, and spontaneous ectopic discharges that are perceived as highly painful in humans (Lindqvist et al., 2000, Janig and Baron, 2003, Black et al., 2008, Ceyhan et al., 2009).

Conclusion

The present data suggest that preventive analgesia by administration of therapies that block the NGF/TrkA axis may be significantly more effective than late administration in reducing the ectopic sprouting as well as pain in a mouse model of bone cancer pain. Whether the

pathological sprouting and neuroma-like formation by sensory and sympathetic nerve fibers is pivotally involved in driving human cancer pain remains unknown but amenable to testing in clinical trials with the several NGF/TrkA blocking strategies that are being developed or already in human clinical trials. Understanding whether similar pathological reorganization of sensory and sympathetic nerve fibers occurs in other malignant and non-malignant chronic pain states is an open and fertile area for both preclinical and clinical research.

Supplementary Material

Refer to Web version on PubMed Central for supplementary material.

Acknowledgments

We thank Marvin Landis and the University of Arizona Information Technology Service for generating the 3D renderings of the innervated bone. This work was supported by the National Institutes of Health grant (NS23970), by the Department of Veterans Affairs, Veterans Health Administration, Rehabilitation Research and Development Service Grants (O4380-I and A6707-R) and by the Calhoun Fund for Bone Pain.

List of references

Averill S, McMahon SB, Clary DO, Reichardt LF, Priestley JV. Immunocytochemical localization of trkA receptors in chemically identified subgroups of adult rat sensory neurons. Eur J Neurosci 1995;7:1484–1494. [PubMed: 7551174]

Ballantyne JC. Pre-emptive analgesia: an unsolved problem. Current Opinion In Anesthesiology 2001;14:499–504. [PubMed: 17019137]

Bamji SX, Majdan M, Pozniak CD, Belliveau DJ, Aloyz R, Kohn J, Causing CG, Miller FD. The p75 neurotrophin receptor mediates neuronal apoptosis and is essential for naturally occurring sympathetic neuron death. J Cell Biol 1998;140:911–923. [PubMed: 9472042]

Bingle L, Brown NJ, Lewis CE. The role of tumour-associated macrophages in tumour progression: implications for new anticancer therapies. J Pathol 2002;196:254–265. [PubMed: 11857487]

Black JA, Nikolajsen L, Kroner K, Jensen TS, Waxman SG. Multiple sodium channel isoforms and mitogen-activated protein kinases are present in painful human neuromas. Ann Neurol 2008;64:644–653. [PubMed: 19107992]

Brainin-Mattos J, Smith ND, Malkmus S, Rew Y, Goodman M, Taulane J, Yaksh TL. Cancer-related bone pain is attenuated by a systemically available delta-opioid receptor agonist. Pain 2006;122:174–181. [PubMed: 16545911]

Brownlow HC, Reed A, Joyner C, Simpson AH. Anatomical effects of periosteal elevation. J Orthop Res 2000;18:500–502. [PubMed: 10937640]

Ceyhan GO, Bergmann F, Kadihasanoglu M, Altintas B, Demir IE, Hinz U, Muller MW, Giese T, Buchler MW, Giese NA, Friess H. Pancreatic neuropathy and neuropathic pain-a comprehensive pathomorphological study of 546 cases. Gastroenterology 2009;136:177–186. e171. [PubMed: 18992743]

Cohen S, Levi-Montalcini R, Hamburger V. A nerve growth factor-stimulating factor isolated from sarcomas 37 and 180. PNAS 1954;40:1014–1018. [PubMed: 16589582]

Devor M. Neuropathic pain: what do we do with all these theories? Acta Anaesthesiol Scand 2001;45:1121–1127. [PubMed: 11683663]

Devor M, Govrin-Lippmann R. Axoplasmic transport block reduces ectopic impulse generation in injured peripheral nerves. Pain 1983;16:73–85. [PubMed: 6191267]

Devor M, Govrin-Lippmann R, Angelides K. Na+ channel immunolocalization in peripheral mammalian axons and changes following nerve injury and neuroma formation. J Neurosci 1993;13:1976–1992. [PubMed: 7683047]

Devor M, Keller CH, Ellisman MH. Spontaneous discharge of afferents in a neuroma reflects original receptor tuning. Brain Res 1990;517:245–250. [PubMed: 2375993]

Devor M, Wall PD. Type of sensory nerve fibre sprouting to form a neuroma. Nature 1976;262:705–708. [PubMed: 958442]

Diamond J, Holmes M, Coughlin M. Endogenous NGF and nerve impulses regulate the collateral sprouting of sensory axons in the skin of the adult rat. J Neurosci 1992;12:1454–1466. [PubMed: 1556603]

England JD, Happel LT, Kline DG, Gamboni F, Thouron CL, Liu ZP, Levinson SR. Sodium channel accumulation in humans with painful neuromas. Neurology 1996;47:272–276. [PubMed: 8710095]

Gallo G, Lefcort FB, Letourneau PC. The trkA receptor mediates growth cone turning toward a localized source of nerve growth factor. J Neurosci 1997;17:5445–5454. [PubMed: 9204927]

Ghilardi JR, Rohrich H, Lindsay TH, Sevcik MA, Schwei MJ, Kubota K, Halvorson KG, Poblete J, Chaplan SR, Dubin AE, Carruthers NI, Swanson D, Kuskowski M, Flores CM, Julius D, Mantyh PW. Selective blockade of the capsaicin receptor TRPV1 attenuates bone cancer pain. J Neurosci 2005;25:3126–3131. [PubMed: 15788769]

Greenfield, GQ. Orthopaedic Pain. In: Boswell, MV.; Cole, BE., editors. Weiner's pain management : a practical guide for clinicians. Boca Raton: CRC Press; 2006. p. 465-476.

Halvorson KG, Kubota K, Sevcik MA, Lindsay TH, Sotillo JE, Ghilardi JR, Rosol TJ, Boustany L, Shelton DL, Mantyh PW. A blocking antibody to nerve growth factor attenuates skeletal pain induced by prostate tumor cells growing in bone. Cancer Res 2005;65:9426–9435. [PubMed: 16230406]

Hongo JS, Laramee GR, Urfer R, Shelton DL, Restivo T, Sadick M, Galloway A, Chu H, Winslow JW. Antibody binding regions on human nerve growth factor identified by homolog- and alanine-scanning mutagenesis. Hybridoma 2000;19:215–227. [PubMed: 10952410]

Honore P, Luger NM, Sabino MA, Schwei MJ, Rogers SD, Mach DB, O'Keefe PF, Ramnaraine ML, Clohisy DR, Mantyh PW. Osteoprotegerin blocks bone cancer-induced skeletal destruction, skeletal pain and pain-related neurochemical reorganization of the spinal cord. Nat Med 2000;6:521–528. [PubMed: 10802707]

Inman VT, Saunders JB. Referred pain from skeletal structures. J Nerve Ment Dis 1944;99:660–667.

Janig W, Baron R. Complex regional pain syndrome: mystery explained? Lancet Neurol 2003;2:687–697. [PubMed: 14572737]

Jimenez-Andrade JM, Mantyh WG, Bloom AP, Xu H, Ferng AS, Dussor G, Vanderah TW, Mantyh PW. A phenotypically restricted set of primary afferent nerve fibers innervate the bone versus skin: Therapeutic opportunity for treating skeletal pain. Bone 2010;46:306–313. [PubMed: 19766746]

Jimenez-Andrade JM, Martin CD, Koewler NJ, Freeman KT, Sullivan LJ, Halvorson KG, Barthold CM, Peters CM, Buus RJ, Ghilardi JR, Lewis JL, Kuskowski MA, Mantyh PW. Nerve growth factor sequestering therapy attenuates non-malignant skeletal pain following fracture. Pain 2007;133:183–196. [PubMed: 17693023]

King T, Vardanyan A, Majuta L, Melemedjian O, Nagle R, Cress AE, Vanderah TW, Lai J, Porreca F. Morphine treatment accelerates sarcoma-induced bone pain, bone loss, and spontaneous fracture in a murine model of bone cancer. Pain 2007;132:154–168. [PubMed: 17706870]

Kryger GS, Kryger Z, Zhang F, Shelton DL, Lineaweaver WC, Buncke HJ. Nerve growth factor inhibition prevents traumatic neuroma formation in the rat. J Hand Surg Am 2001;26:635–644. [PubMed: 11466637]

Lawson SN, Perry MJ, Prabhakar E, McCarthy PW. Primary sensory neurones: neurofilament, neuropeptides, and conduction velocity. Brain Res Bull 1993;30:239–243. [PubMed: 7681350]

Lawson SN, Waddell PJ. Soma neurofilament immunoreactivity is related to cell size and fibre conduction velocity in rat primary sensory neurons. J Physiol 1991;435:41–63. [PubMed: 1770443]

Lindqvist A, Rivero-Melian C, Turan I, Fried K. Neuropeptide- and tyrosine hydroxylase-immunoreactive nerve fibers in painful Morton's neuromas. Muscle Nerve 2000;23:1214–1218. [PubMed: 10918258]

Lindsay TH, Jonas BM, Sevcik MA, Kubota K, Halvorson KG, Ghilardi JR, Kuskowski MA, Stelow EB, Mukherjee P, Gendler SJ, Wong GY, Mantyh PW. Pancreatic cancer pain and its correlation

with changes in tumor vasculature, macrophage infiltration, neuronal innervation, body weight and disease progression. Pain 2005;119:233–246. [PubMed: 16298491]

Mach DB, Rogers SD, Sabino MC, Luger NM, Schwei MJ, Pomonis JD, Keyser CP, Clohisy DR, Adams DJ, O'Leary P, Mantyh PW. Origins of skeletal pain: sensory and sympathetic innervation of the mouse femur. Neuroscience 2002;113:155–166. [PubMed: 12123694]

Madduri S, Papaloizos M, Gander B. Synergistic effect of GDNF and NGF on axonal branching and elongation in vitro. Neurosci Res 2009;65:88–97. [PubMed: 19523996]

Mantyh PW. Cancer pain and its impact on diagnosis, survival and quality of life. Nat Rev Neurosci 2006;7:797–809. [PubMed: 16988655]

Mercadante S. Malignant bone pain: pathophysiology and treatment. Pain 1997;69:1–18. [PubMed: 9060007]

Mercadante S, Arcuri E. Breakthrough pain in cancer patients: pathophysiology and treatment. Cancer Treat Rev 1998;24:425–432. [PubMed: 10189409]

Mercadante S, Villari P, Ferrera P, Casuccio A. Optimization of opioid therapy for preventing incident pain associated with bone metastases. J Pain Symptom Manage 2004;28:505–510. [PubMed: 15504626]

Normann SJ. Macrophage infiltration and tumor progression. Cancer Metastasis Rev 1985;4:277–291. [PubMed: 3907821]

Nystrom B, Hagbarth KE. Microelectrode recordings from transected nerves in amputees with phantom limb pain. Neurosci Lett 1981;27:211–216. [PubMed: 7322453]

Peters CM, Ghilardi JR, Keyser CP, Kubota K, Lindsay TH, Luger NM, Mach DB, Schwei MJ, Sevcik MA, Mantyh PW. Tumor-induced injury of primary afferent sensory nerve fibers in bone cancer pain. Exp Neurol 2005;193:85–100. [PubMed: 15817267]

Pezet S, McMahon SB. Neurotrophins: mediators and modulators of pain. Annu Rev Neurosci 2006;29:507–538. [PubMed: 16776595]

Pogatzki-Zahn EM, Zahn PK. From preemptive to preventive analgesia. Curr Opin Anaesthesiol 2006;19:551–555. [PubMed: 16960490]

Portenoy RK. Managing cancer pain poorly responsive to systemic opioid therapy. Oncology 1999;13:25–29. [PubMed: 10356695]

Portenoy RK, Hagen NA. Breakthrough pain: definition, prevalence and characteristics. Pain 1990;41:273–281. see comments. [PubMed: 1697056]

Portenoy RK, Lesage P. Management of cancer pain. Lancet 1999;353:1695–1700. [PubMed: 10335806]

Schmidt RE, Dorsey DA, Selznick LA, DiStefano PS, Carroll SL, Beaudet LN, Roth KA. Neurotrophin sensitivity of prevertebral and paravertebral rat sympathetic autonomic ganglia. J Neuropathol Exp Neurol 1998;57:158–167. [PubMed: 9600208]

Schwei MJ, Honore P, Rogers SD, Salak-Johnson JL, Finke MP, Ramnaraine ML, Clohisy DR, Mantyh PW. Neurochemical and cellular reorganization of the spinal cord in a murine model of bone cancer pain. J Neurosci 1999;19:10886–10897. [PubMed: 10594070]

Sevcik MA, Ghilardi JR, Halvorson KG, Lindsay TH, Kubota K, Mantyh PW. Analgesic efficacy of bradykinin B1 antagonists in a murine bone cancer pain model. J Pain 2005a;6:771–775. [PubMed: 16275602]

Sevcik MA, Ghilardi JR, Peters CM, Lindsay TH, Halvorson KG, Jonas BM, Kubota K, Kuskowski MA, Boustany L, Shelton DL, Mantyh PW. Anti-NGF therapy profoundly reduces bone cancer pain and the accompanying increase in markers of peripheral and central sensitization. Pain 2005b; 115:128–141. [PubMed: 15836976]

Sevcik MA, Luger NM, Mach DB, Sabino MA, Peters CM, Ghilardi JR, Schwei MJ, Rohrich H, De Felipe C, Kuskowski MA, Mantyh PW. Bone cancer pain: the effects of the bisphosphonate alendronate on pain, skeletal remodeling, tumor growth and tumor necrosis. Pain 2004;111:169–180. [PubMed: 15327821]

Shelton DL, Zeller J, Ho WH, Pons J, Rosenthal A. Nerve growth factor mediates hyperalgesia and cachexia in auto-immune arthritis. Pain 2005;116:8–16. [PubMed: 15927377]

Small JR, Scadding JW, Landon DN. A fluorescence study of changes in noradrenergic sympathetic fibres in experimental peripheral nerve neuromas. J Neurol Sci 1990;100:98–107. [PubMed: 2089147]

Sung JH, Mastri AR. Aberrant peripheral nerves and microneuromas in otherwise normal medullas. J Neuropathol Exp Neurol 1983;42:522–528. [PubMed: 6310057]

van den Beuken-van Everdingen M, de Rijke J, Kessels A, Schouten H, van Kleef M, Patijn J. Prevalence of pain in patients with cancer: a systematic review of the past 40 years. Ann Oncol. 2007

Woolf CJ, Chong MS. Preemptive analgesia--treating postoperative pain by preventing the establishment of central sensitization. Anesth Analg 1993;77:362–379. [PubMed: 8346839]

Yen LD, Bennett GJ, Ribeiro-da-Silva A. Sympathetic sprouting and changes in nociceptive sensory innervation in the glabrous skin of the rat hind paw following partial peripheral nerve injury. J Comp Neurol 2006;495:679–690. [PubMed: 16506190]

Abbreviations

CGRP	Calcitonin gene related peptide
CRPS	Complex regional pain syndrome
GFP	Green fluorescent protein
HBSS	Hank's buffered sterile saline
NF200	200 kD neurofilament H
NGF	Nerve growth factor
PBS	Phosphate buffered saline
TH	Tyrosine hydroxylase
TrkA	Tropomyosin receptor kinase A
μCT	Micro-computed tomography

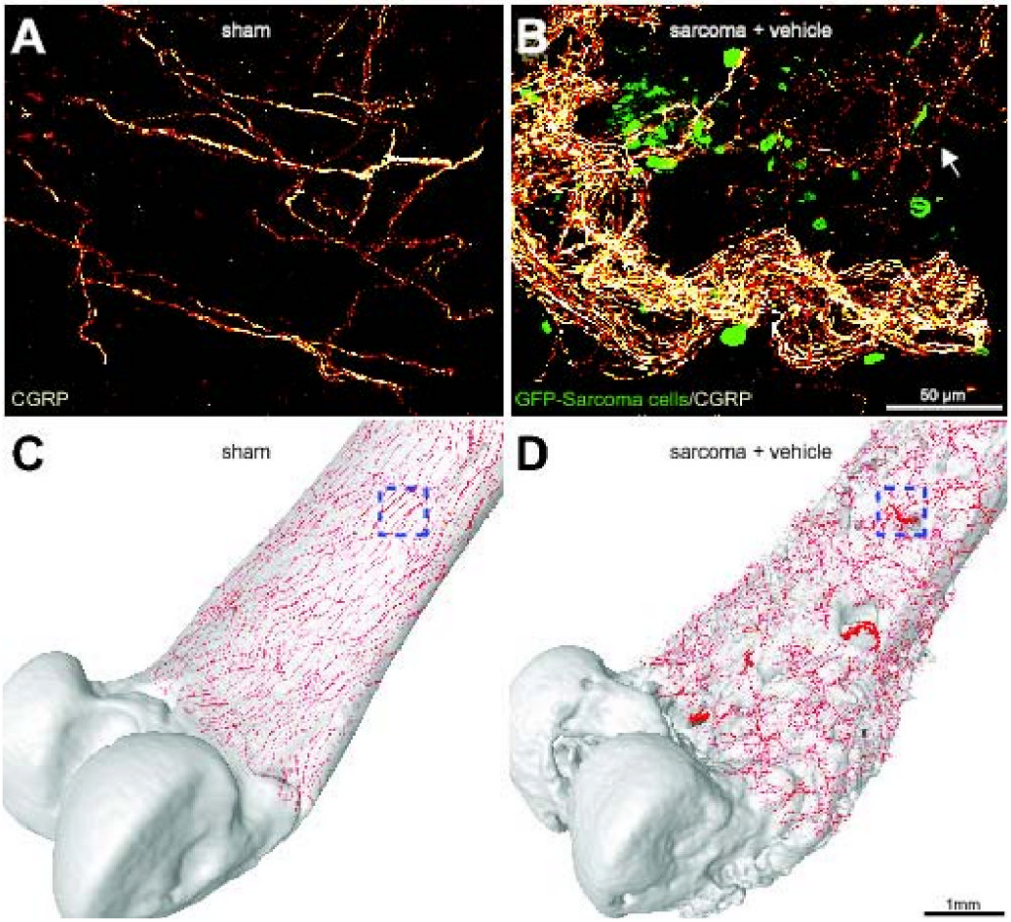

Figure 1.

Sensory nerve fibers sprout and form neuroma-like structures as tumor cells invade the periosteum of the bone. Confocal images of non-decalcified whole mount preparations of the femoral periosteum from sham + vehicle (A) or sarcoma + vehicle mice (B) showing $CGRP^+$ nerve fibers and GFP^+ sarcoma cancer cells. When GFP^+ tumor cells invade the periosteum, they induce ectopic sprouting of $CGRP^+$ sensory fibers (B, arrow) and the formation of neuroma-like structures. Confocal images of periosteum (approximately 70 μm in thickness) were acquired from whole mount preparations and projected into a Z-stack from 280 optical sections at 0.25 μm intervals with a 40× objective. Four Z-stack images from sham or sarcoma + vehicle mice were tiled and overlayed (to scale) on a three-dimensional micro-CT rendering of a sham femur (C) or sarcoma + vehicle femur (D), respectively, using Amira software. The boxed areas in (C) and (D) correspond to the confocal images in (A) and (B), respectively. Note that the tumor-injected femur (D) has severe cortical bone deterioration and a pathological reorganization of CGRP nerve fibers (in red) compared to the sham bone (C).

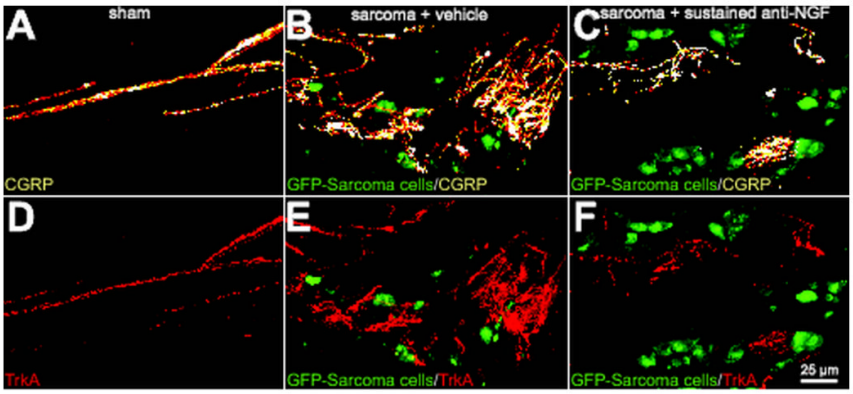

Figure 2.

Preventive sequestration of NGF reduces CGRP$^+$ and TrkA$^+$ nerve fiber sprouting and the formation of neuroma-like structures in the periosteum of tumor-injected mice. Representative confocal images of femoral sections from sham + vehicle (A, D), sarcoma + vehicle (B, E), and sarcoma + early/sustained anti-NGF (C, F) mice. Decalcified bone sections were double-immunostained with an antibody against CGRP (orange in A, B, C) and an antibody against TrkA (cognate receptor for NGF, red in D, E, F). Confocal images were acquired in the proximal metaphyseal periosteum (~2 mm below the growth plate) using a sequential acquisition mode to reduce bleed-through. Note that at day 20 post-injection there is remarkable sprouting by CGRP$^+$ nerve fibers in sarcoma + vehicle mice (B) and that nearly all the sprouted CGRP$^+$ nerve fibers also express TrkA (E). Nerve fibers that undergo sprouting have a remarkable pathological and disorganized morphology as compared to nerve fibers innervating sham bones. Preventive sequestration of NGF (10 mg/kg; i.p., given at days 6, 12, and 18 post cell injection) significantly reduces the pathological tumor-induced reorganization of sensory CGRP$^+$ (C) and TrkA$^+$ (F) nerve fibers. Confocal images were acquired from bone sections (20 μm in thickness) and were projected from 120 optical sections at 0.25μm intervals with a 40× objective.

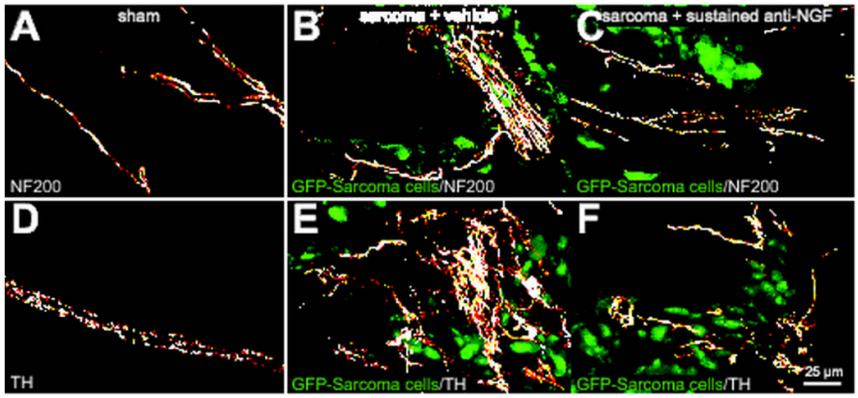

Figure 3.

Preventive sequestration of NGF inhibits tumor-induced nerve fiber sprouting of $NF200^+$ sensory nerve fibers and TH^+ sympathetic nerve fibers. Representative confocal images of decalcified bone sections from sham + vehicle (A, D), sarcoma + vehicle (B, E), and sarcoma + early/sustained anti-NGF treated mice (C, F). Decalcified bone sections were separately stained with an antibody against 200kD Neurofilament (NF200, a marker of myelinated sensory nerve fibers, white in A, B, C) and an antibody against Tyrosine Hydroxylase (TH, a marker for sympathetic nerve fibers, white in D, E, F). Note that at day 20 post cell injection, GFP^+ tumor cells (green) induce ectopic sprouting and formation of neuroma-like structures by $NF200^+$ and TH^+ nerve fibers in the periosteum (B, E). Previous data has shown that nearly all sympathetic TH^+ nerve fibers and a significant population of $NF200^+$ sensory nerve fibers express TrkA (Averill et al., 1995, Schmidt et al., 1998) Early/sustained anti-NGF therapy (10 mg/kg; i.p., given at days 6, 12, and 18 post cell injection) largely blocks the tumor-induced remodeling of TrkA-expressing $NF200^+$ and TH^+ nerve fibers (C, F). In all cases, images were acquired in the proximal metaphyseal periosteum (~2 mm below the growth plate). Confocal images were acquired from bone sections (30 μm in thickness) and were projected from 120 optical sections at 0.25 μm intervals with a 40× objective.

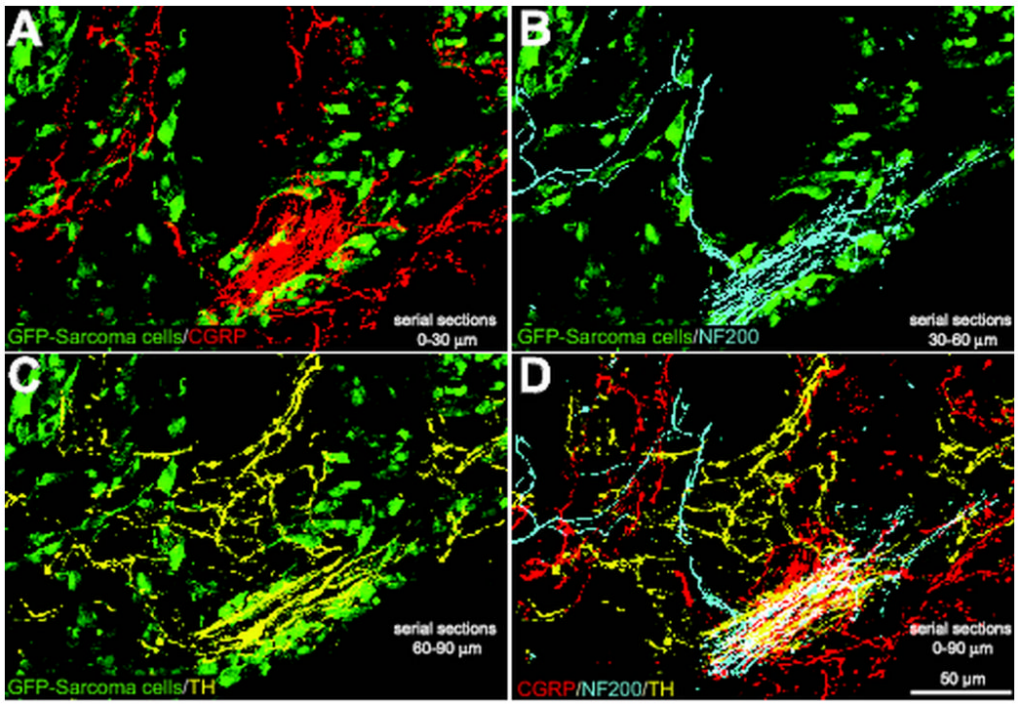

Figure 4.

Sensory and sympathetic nerve fibers are observed in the same neuroma-like structures in tumor-bearing mice. Confocal images of serial sections of bone (each 30 µm apart) immunostained with CGRP (serial section 1, red, A), NF200 (serial section 2, blue, B), and TH (serial section 3, yellow, C) from a tumor-bearing mouse. At 20 days post-injection, GFP^+ cancer cells (green, A, B, C) had induced dramatic sprouting and formation of neuroma-like structures by $CGRP^+$, $NF200^+$, and TH^+ nerve fibers in the periosteum/cortical bone interface. Note that when the confocal images of nerve fibers are merged (D), all three fiber types appear to be present in the same neuroma-like structure, which appears white in (D). The GFP background in A to C was acquired from the middle section (serial section 2). The merged image is a Z-stack of confocal images projected from 360 optical sections at 0.25µm intervals with a 40× objective.

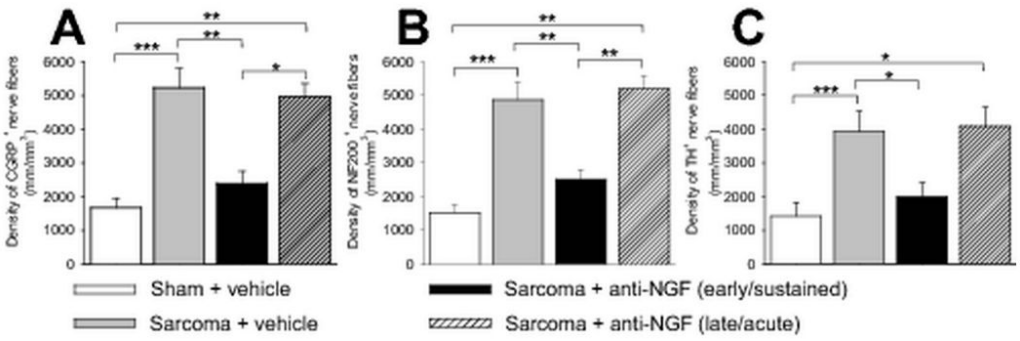

Figure 5.

Early, but not late administration of NGF sequestering therapy reduces sarcoma-induced nerve sprouting of $CGRP^+$, $NF200^+$, and TH^+ nerve fibers. At day 20 post cell injection, the density of $CGRP^+$ (A), $NF200^+$ (B), and TH^+ (C) nerve fibers is significantly greater in sarcoma + vehicle-treated mice compared to sham + vehicle-treated mice. This tumor-induced nerve sprouting is significantly attenuated by early/sustained (10 mg/kg; i.p., given at days 6, 12, and 18 post cell injection), but not by late/acute (10 mg/kg; i.p., given at day 18 post cell injection) administration of anti-NGF. Nerve fiber density was determined by measuring the total length of nerve fibers per unit area in the periosteum. Confocal images from three decalcified bone sections per animal and per marker were acquired in the proximal metaphyseal periosteum (~2 mm below the growth plate) and used to determine the length of nerve fibers. Both imaging acquisition and analysis were performed in a blinded fashion. Brackets indicate the groups being compared. *$p<0.05$, **$p<0.01$, ***$p<0.001$. Bars represent the mean ± SEM. The number of animals was n=8 for sham, n=9 for sarcoma + vehicle, n=9 for sarcoma + early/sustained anti-NGF, and n=7 for sarcoma + late/acute anti-NGF.

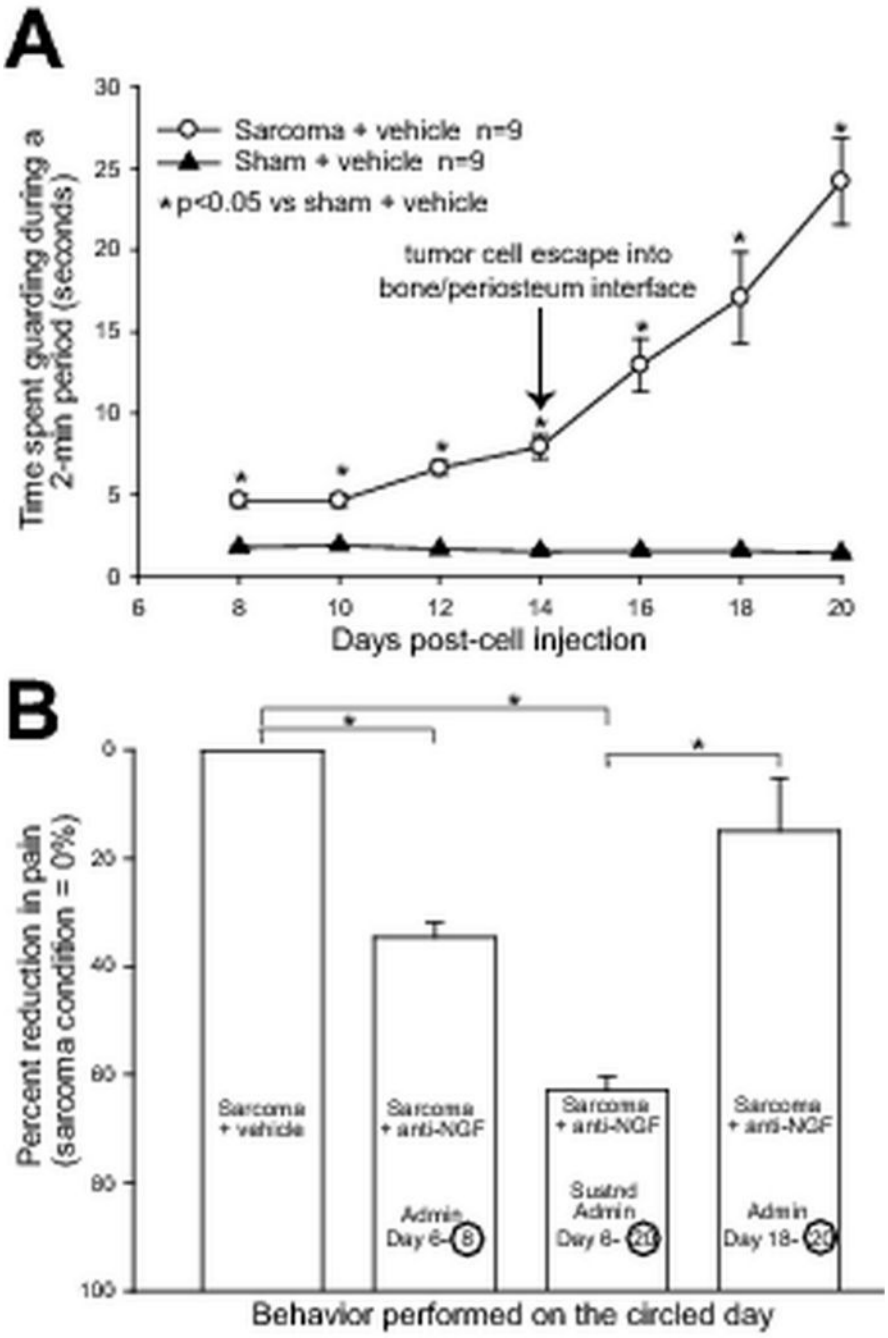

Figure 6.

Early, but not late administration of NGF sequestering therapy reduces late stage cancer pain behaviors. Injection of GFP^+ sarcoma cells into the intramedullary space of the femur results in significantly greater pain behaviors compared to sham mice (A) from day 8 until day 20 post cell injection. Note that at day 14 there is a rapid escalation of pain behaviors, which corresponds to the invasion and growth of GFP^+ cancer cells within the periosteum. We hypothesize that the escalation of the pain behaviors in part results from significant sprouting and formation of neuroma-like structures by $CGRP^+$ sensory (Fig. 2), $NF200^+$ sensory (Fig. 3), and TH^+ sympathetic (Fig. 3) nerve fibers in the periosteum. In concordance with our anatomical findings, anti-NGF therapy significantly reduces cancer

pain behaviors only if this therapy is administered before sprouting and neuroma formation occur, in either an early/acute (administration at day 6, pain behaviors evaluated at day 8), or an early/sustained administration at (days 6, 12, and 20, pain behaviors evaluated at day 20) fashion (B). In contrast, NGF administered at late time points (administration at day 18, pain behaviors evaluated at day 20), when nerve sprouting and neuroma-like structures have already formed, does not significantly reduce cancer pain behaviors. Each point or bar represents the mean ± SEM. Brackets indicate the groups being compared. *$p<0.01$. The number of animals was n=9 for sarcoma + vehicle, n=7 for sarcoma + early/acute administration of anti-NGF, n=7 for sarcoma + early/sustained administration of anti-NGF, and n=9 for sarcoma + late/acute administration of anti-NGF.

Table 1
Anti-NGF does not affect the non-tumor bearing bone's normal innervation

Marker	Sham + vehicle Density of nerve fibers (mm/mm^3)	Contralateral + early/sustained anti-NGF Density of nerve fibers (mm/mm^3)
CGRP	1669 ± 288 (n=8)	1594 ± 86 (n=6)
NF200	1535 ± 215 (n=8)	1620 ± 81 (n=6)
TH	1053 ± 200 (n=8)	1112 ± 96 (n=6)

Mean Values ± SEM

Non significant differences following Mann-Whitney non-parametric t-tests

p-values are: CGRP p=.945; NF200 p=1.00; TH p=.662.